Study of the tunable mechanical and swelling properties of magnetic sensitive calcium alginate nanocomposite hydrogels

Alberto Varela-Feijoo, Alain Ponton

Rheologica Acta
https://doi.org/10.1007/s00397-023-01384-1

ORIGINAL CONTRIBUTION

Study of the tunable mechanical and swelling properties of magnetic sensitive calcium alginate nanocomposite hydrogels

Alberto Varela-Feijoo[1,2] · **Alain Ponton**[1]

Received: 2 August 2022 / Revised: 11 January 2023 / Accepted: 11 January 2023

Abstract

Nanocomposite hydrogels were elaborated by the addition of citrated magnetic nanoparticles (MNPs) in sodium alginate aqueous solutions ionically crosslinked by in situ release of calcium ions from calcium carbonate ($CaCO_3$) with gradual hydrolysis of D-glucono-δ lactone (GDL). The sol-gel transition was studied by time-resolved mechanical spectroscopy (TRMS) in the linear viscoelastic region. The power law frequency dependence of the storage and loss moduli allowed to determine the gelation time (t_g), the power law relaxation exponent (Δ), and the gel stiffness (S) at the critical gel (gel at t_g) for different calcium and MNP concentrations. The effect of an applied magnetic field on these parameters was also studied for the first time. The obtained results show an effect of the concentration of both calcium and MNPs on the kinetics (t_g) and properties at the critical gel (S and Δ) obtaining faster kinetics and harder critical gels for higher calcium and lower MNP concentrations. Moreover, the application of the magnetic field allows to modulate the viscoelastic properties before the gel point, but no effect was observed on the structural properties of the critical gel. Finally, this work highlights how the shear viscoelastic, compressive, and swelling properties of totally gelled nanocomposite hydrogels can be successfully modulated when MNPs are introduced in the calcium alginate matrices with a good agreement between all these properties and with the properties of the critical gels.

Keywords Hydrogels · Magnetic nanocomposite · Viscoelasticity · Compression · Swelling · Sol-gel transition

Introduction

Hydrogels are three-dimensional (3D), insoluble, crosslinked polymer networks combining liquid-like and solid-like properties with different interesting relaxation properties. They are able to retain a large amount of water in their swollen state due to hydrophilic functional groups attached to the polymer backbone while their resistance to dissolution arises from crosslinks between polymer chains (Varaprasad et al. 2017). Water inside the hydrogel allows free diffusion of some solute molecules, while the polymer serves as a matrix to hold water together (Okay 2010). Hydrogels have a variety of properties, such as absorption capacity, swelling behavior, stability/degradability, bioactivity, permeability, and mechanical, optical, and surface properties, which make them promising materials for diverse applications (Patel and Thareja 2022). In particular, a lot of studies in the literature are concerned by the elaboration of calcium alginate hydrogels by different methodologies and with different shapes such as films (Li et al. 2016), beads (Leong et al. 2016), or disks (Maki et al. 2011; Growney Kalaf et al. 2016) in view of their multiple applications.

In some cases, the properties of hydrogels can be modulated by external stimuli including heat, light, magnetic or electric fields, chemical agents, and pH (Ahn et al. 2008; Stuart et al. 2010). The addition of fillers to hydrogels to elaborate hybrid organic-inorganic composite materials is another interesting approach in order to modulate their properties (Schexnailder and Schmidt 2009). The size of fillers has a high effect on the resulting properties of the composites. This is because surface interactions with the matrix, adhesion, particle motion, dispersion, bonding, etc., increase with a decrease in filler size, making the choice of nanofillers a promising approach. More precisely, the assembly of inorganic nanofillers in hydrogel matrices to elaborate hybrid nanocomposites has

✉ Alain Ponton
alain.ponton@univ-paris-diderot.fr

[1] Université Paris Cité, CNRS, Matière et systèmes complexes, F-75013 Paris, France

[2] Université Paris Saclay, INRAE, AgroParisTech, UMR SayFood, 91120 Palaiseau, France

Published online: 02 February 2023

become increasingly attractive in recent years (Sanchez et al. 2005; George and Ishida 2018).

One particular case is the elaboration of nanocomposites by introducing metallic nanoparticles such as Fe, Co, Ni, and their oxides, Fe_3O_4, Fe_2O_3, $CoFe_2O_3$, FePt, CoPt, etc., which show unique magnetic properties allowing to obtain excellent stimuli-responsive nanocomposite hydrogels (Sarkar et al. 2012). The interesting properties of such nanocomposites come from the combination of superparamagnetic properties of magnetic nanoparticles (MNPs) with no remanence and high saturation magnetization and polymer matrices of different natures (Thévenot et al. 2013; Ridi et al. 2014).

Although much research has been devoted to magnetic composite hydrogels, little information is available on the time-dependent viscoelastic and structural properties in relationship with the elaboration or under applied magnetic field. The present work addresses this problem and reports the elaboration of nanocomposite hydrogels based on sodium alginate aqueous solutions ionically crosslinked by in situ calcium release from insoluble $CaCO_3$ salt and the addition of MNP aqueous dispersions. The sol-gel transition is firstly studied to evaluate the effect of the calcium, MNP concentrations, and applied magnetic field by time-resolved mechanical spectroscopy (TRMS). The mechanical properties of the totally gelled nanocomposites are secondly evaluated by oscillatory shear rheology and uniaxial compression tests and swelling properties are also investigated.

Materials and methods

Magnetic nanoparticles (MNPs)

Synthesis

Maghemite MNPs were prepared by the co-precipitation method proposed by R. Massart (1982). Briefly, 214 mL of aqueous solution of ferric chloride 0.43M ($FeCl_3.6H_2O$, SIGMA-ALDRICH, ≥99%) was prepared in a 3-necked flask. Freshly dissolved ferrous chloride 0.4M ($FeCl_2.4H_2O$, Across Organics, ≥99%) in 35 mL of 2M HCl (aq) was dropped in the 3-necked flask under stirring at room temperature. When the iron precursors were homogeneously mixed, 71 mL of NH_3 (Technic 28-30% v/v) was added and the mixture was maintained under stirring at 400 rpm for 30 min to obtain magnetite MNPs.

The obtained mixture was then decanted on a magnetic plate, recovering the precipitate composed of MNPs and removing the liquid supernatant. Following, magnetite nanoparticles (α-Fe_3O_4) were oxidized into maghemite (γ-Fe_2O_3) by adding nitric acid (1M) and boiling iron nitrate ($Fe(NO_3)_3$) aqueous solution and stirred for 1 h at 90°C. After equilibration at room temperature, the resulting precipitate was washed three times with acetone and two times with ether to obtain bare maghemite MNPs. The as-produced MNPs tend to agglomerate and to precipitate due to magnetic dipole, van der Waals forces, and high energy surface when they were dispersed in water. To obtain stable colloidal dispersions of MNPs, repulsive electrostatic forces were introduced by the adsorption of citrated ions on the surface of the MNPs. For such purpose, MNPs were dispersed in 71 mL of pure water and 2 g of sodium citrate (SIGMA-ALDRICH, ≥99%) and left for 30 min under mechanical stirring at 80°C. After cooling down at room temperature and decantation on the magnetic plate, the washing procedure was repeated with acetone and ether. Finally, the citrated maghemite MNPs were dispersed in 25 mL of pure water to obtain a citrated ferrofluid with a concentration in MNPs of 18% w/w.

Transmission electron microscopy (TEM)

TEM measurement was performed on a Tecnai12 transmission electron microscope. A diluted dispersion of MNPs was prepared by mixing a calculated amount of ferrofluid with pure water to obtain the final concentration of 0.05% w/w. The sample was then introduced 10 min on the ultrasonic bath to ensure a good dispersion and a small droplet was placed in a copper grid. The sample was then dried in a vacuum oven and the grid was inserted in the TEM device.

Zeta potential and size distribution by dynamic light scattering (DLS)

The measurements were performed using the Zetasizer Nano ZS (Malvern instruments). For the determination of the hydrodynamic diameter, 1 mL of diluted in water (η=0.89 mPa.s at 25°C) ferrofluid with a concentration of 0.01% w/w was placed in a cubic cuvette and the measurement of temporal fluctuation of the scattering intensity with a recorded signal during 60 s with a count rate of 360 kcounts s^{-1} was performed at the constant temperature of 25°C. Through a process of correlating the intensity of scattered photons at various time points, the corresponding decay in correlation is used to determine the diffusion rate for the particles. More precisely, the hydrodynamic diameter of MNPs was calculated by the fitting of the correlation function with an algorithm as the commonly used constrained regularization method for inverting data, which assumes a logarithmic distribution (Ostolska and Wiśniewska 2014).

For the determination of the zeta potential, the measurements were performed for MNP aqueous dispersion with a concentration of 0.2% w/w at 25°C in a folded capillary cell. The electrophoretic mobility (U_E) of charged MNPs was determined from particle velocity under an applied electric field. The zeta potential (ζ) was then

calculated from the obtained electrophoretic mobility (U_E), by using Henry's equation (Kaszuba et al. 2010).

$$\zeta = \frac{3\eta U_E}{2\varepsilon f(ka)} \quad (1)$$

where ε is the dielectric constant and $f(ka)$ is Henry's function with a value of 1.5 following the Smoluchowski approximation for aqueous media and moderate electrolyte concentration (Hunter 1981).

Hydrogels and nanocomposite hydrogels

Magnetization

The magnetization as a function of the applied magnetic field was measured with a vibrating sample magnetometer (VSM). The studied samples are mixtures of sodium alginate solution with citrated MNPs with two volume fractions ($\Phi_{MNPs} = 0.5$ and 1% v/v), a nanocomposite hydrogel to prove that crosslinking has no effect on magnetic properties and dried powder of MNPs to estimate the saturation magnetization of pure MNPs. To perform the measurement, a small amount of sample was weighted and introduced in a glass cup connected to a vibration unit and a continuous magnetic field was applied between −1600 and +1600 kA m^{-1} with an electromagnet in an environmental controlled area at 293K. The magnetization was deduced from the magnetic flux generated by the sample by tracking the voltage generated by this varying magnetic flux in the coils.

Elaboration of hydrogels and nanocomposite hydrogels

Powder of low molecular weight sodium alginate (MP Biomedicals) of cream color with a determined humidity of 8% w/w was briefly characterized in the laboratory. The molecular weight was determined by viscometry measurements obtaining $M_v = 10^5$ g mol^{-1}. Moreover, the FTIR spectra were recorded in a Bruker Equinox spectrometer in the range 400–4000 cm^{-1}. KBr pellet of dried sodium alginate powder was prepared, and the spectra were recorded in transmission mode at room temperature (see Fig. S1 in the supporting information). The relative content of mannuronate (M) to guluronate (G) was estimated by the methodology proposed by Sakugawa et al. (2004) and found to be M/G = 0.58.

Mother solution of sodium alginate with a concentration of 40 g L^{-1} was prepared in a 100-mL Fisherbrand glass bottle. The sodium alginate powder was mixed with 50 mL of pure water under mechanical stirring of 400 rpm for 14 h. The obtained viscous and homogeneous solution was stored in the fridge and used for a maximum of 10 days.

Calcium alginate hydrogels were elaborated by ionic crosslinking with calcium bivalent cations. A direct mixing of alginate and calcium cations rarely produces homogeneous hydrogels due to the very rapid and irreversible binding of such ions (Draget and Taylor 2011). A controlled introduction of crosslinking ions to produce homogeneous hydrogels was possible using an in situ two-step method as proposed by Ingar Draget et al. (1990). The use of calcium carbonate ($CaCO_3$) as the source of calcium presents the advantage of requiring less quantity of chemical products than with other alternatives such as the complexation of $CaCl_2$-EDTA (Yamamoto et al. 2019). Firstly, the insoluble powder was homogeneously dispersed in the sodium alginate solution. Afterwards, a freshly prepared aqueous solution of glucono-delta-lactone (GDL) was added inducing the slow dissolution of $CaCO_3$ by the release of H^+ from the hydrolysis of GDL. The selected alginate concentration was 18 g L^{-1} low enough to ensure homogeneous dispersion of MNPs and $CaCO_3$ particles and high enough to obtain appropriate mechanical properties at the totally gelled state. Different molar ratios between added calcium and carboxylic groups in the sodium alginate chains ($R_{Ca} = [Ca^{2+}]/[COO^-]$) were fixed to 0.2, 0.3, and 0.4 since values lower than 0.2 lead to extremely soft hydrogels and values higher than 0.4 have shown to not increase significantly the mechanical properties of the totally gelled hydrogels.

The precise experimental protocol consisted in the dispersion of calculated weights of $CaCO_3$ powder in a sodium alginate aqueous solution during 10 min under mechanical stirring and 10 min in the ultrasonic bath obtaining the pre-gel system. Freshly prepared aqueous solution of GDL with the molar ratio $([GDL])/[CaCO_3] = 2$) was then quickly added to the pre-gel system under mechanical stirring to induce the slow dissolution of $CaCO_3$. Nanocomposite hydrogels were elaborated with a fixed molar ratio ($R_{Ca} = 0.4$) since the lower values of R_{Ca} lead to very long gelation times when the MNPs were added. The selected volume fractions of MNPs were $\Phi_{MNPs} = 0.5\%$ and $\Phi_{MNPs} = 1\%$ to obtain macroscopically homogeneous nanocomposites based on a previous study (Roger et al. 2015). For such cases, a calculated mass of citrated ferrofluid was introduced and mixed by mechanical stirring in the pre-gel system before the addition of GDL following the scheme of Fig. 1.

Study of the sol-gel transition

The study of the sol-gel transition by creep experiment (measurement of shear stress as a function of time under applied constant shear strain) is not appropriate for samples for which the gelation process cannot be quenched at different times. Therefore, it was performed according to the mechanical definition of the critical gel proposed by Winter and Chambon (1988). Briefly, this approach is based on the experimental finding that both elastic (G') and loss (G'') have a power law frequency dependence with the same exponent

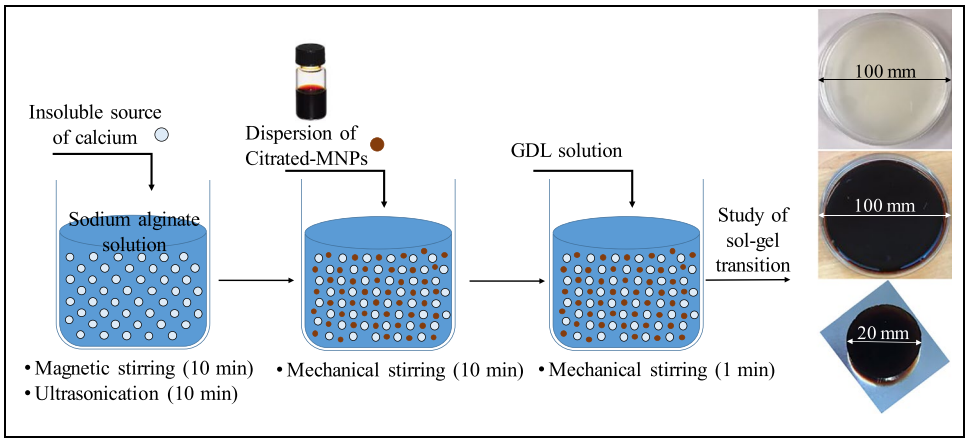

Fig. 1 Schematic representation of the elaboration of calcium alginate nanocomposite hydrogels

(Δ) at the gel point and the ratio of both moduli is independent of the frequency. Consequently, the plot of G''/G' as a function of time for the different frequencies allows to determine the gelation time (t_g) from the intersection point of all the curves. The relaxation exponent (Δ) and the gel stiffness (S) can be then deduced from the values of G' and G'' at t_g. A more detailed description could be found in supporting information. The theoretical values of Δ are between 0 and 1. The case of $\Delta = 0$ corresponds to the limiting behavior of a Hookean solid (the relaxation modulus is a constant) while the restriction of Δ to values less than unity is necessary to assure a diverging zero-shear viscosity at the gel point.

This experimental study of the sol-gel transition is known as time-resolved mechanical spectroscopy (TRMS). It was performed in the present study with a torque-controlled rheometer MARS II (Thermo Fischer Scientific) fitted with a magnetic system developed in the Matière et systèmes complexes (MSC) laboratory (Galindo-Gonzalez et al. 2016). A cone-and-plate geometry (60 mm in diameter and an angle of 1°) made of nonmagnetic material was selected for all the rheological measurements. Two coils placed on both sides of the cone-plate geometry allow to create a homogeneous magnetic field perpendicular to the shear by circulating an electric current through the coils. The temperature of the sample was controlled by a water circulation at 25.0±0.1°C under the plate.

To perform the measurement, the pre-gel sample just after the addition of GDL was mixed for 40 s before being loaded on the plate. The protocol to obtain time-resolved data consists in the application of successive frequency sweeps between 0.2 and 3 Hz at a constant stress amplitude of 1 Pa within the linear viscoelastic domain (LVD). The TRMS experiment protocol requires that the time evolution of the rheological properties of the samples remain negligible compared to the period (t_{exp}) of each frequency sweep. This hypothesis can experimentally be checked in terms of a mutation number N_{mu} which quantifies the change of a dynamical rheological property during an experiment (Mours and Winter 1994). For a gelation experiment, Winter et al. (1988) found that a sample can be considered quasi-stable if $N_{mu} < 0.15$. This condition is verified for all performed measurements in this study by TRMS.

To minimize water evaporation, a solvent trap was used to maintain a humid atmosphere surrounding the sample. For the nanocomposite samples, a continuous magnetic field was applied between 0 and 13.9 kA m^{-1} during the rheological measurements.

Study of totally gelled hydrogels

Forty grams of the pre-gel system with $R_{Ca} = 0.4$ and two volume fractions of MNPs ($\Phi_{MNPs} = 0.5\%$ and 1%) were prepared following the protocol described in the "Elaboration of hydrogels and nanocomposite hydrogels" section, placed in a sealed petri dish with a diameter of 10 cm just after adding GDL solution and left for 16 h at 25°C (Fig. 1). Solid hydrogel was obtained and cylindrical disks with a diameter of 20 mm and a variable thickness between 5 and 7 mm were prepared with a cutter tool punch to perform the experiments as explained below.

Shear rheology

Oscillatory shear measurements were performed using MARS II rheometer with a plate and plate geometry of 20 mm of diameter. The gel disk was placed on the lower plate and the gap was selected manually. The contact between the upper plate and the gel disk was considered to be obtained when a small compressive pre-load of 0.02N was reached. This value was reinitialized to zero before the shear experiment. Elastic (G') and loss (G'') moduli were measured during the application of a sinusoidal strain sweep between 10^{-3} and 100 at a constant frequency ($f = 1$ Hz). Temperature was controlled on the lower plate by water circulation at 25.0±0.1°C.

Uniaxial compression

Uniaxial compression tests were performed using the normal force sensor of the MARS II rheometer with a plate and plate geometry of 20 mm of diameter. The prepared cylindrical disks were placed on the lower plate. As for shear rheology, the contact between the upper plate and cylindrical disks was considered to be obtained when a small compressive pre-load of 0.02N was reached. This value was reinitialized to zero before uniaxial compression. Strain was varied between 0 and 40% for all the measurements with a test speed of 1.8 mm min^{-1} and the value of stress was recorded every 0.5% of strain. Temperature was controlled on the lower plate by water flow at 25.0±0.1°C. Measurements were performed by triplicate for three different samples and average values with their mean deviation were calculated for the analyzed experimental data.

Syneresis

It is known that the interaction between alginate and Ca^{2+} ions during gel formation results in the shrinkage of the gel due to the discharge of water (syneresis) from the gel. Since this mechanism is slightly related with the structure of the hydrogel network, the different amounts of water released from the sample during the gelation were measured as the difference of weight between the pre-gel system and the obtained hydrogels at $t = 16$h after gentle surface wiping using absorbent paper.

Swelling

The capability of the hydrogels to absorb water was studied through a swelling study of the as-prepared cylindrical disks. They were individually introduced in plastic cups filled with 20 mL of pure water and weighted at different times after gentle surface wiping using absorbent paper. The water content after each measurement was calculated using the following equation:

$$Q(\%) = \frac{W_s(t) - W_0}{W_0} \times 100 \quad (2)$$

where $W_s(t)$ is the weight of a swollen disk at time t and W_0 is the initial weight of the as-prepared disk just before immersion in water. Measurements were performed by triplicate for three different samples and average values were calculated for the analyzed experimental data. After the equilibrium swelling degree (Q_e) is achieved, uniaxial compression tests were performed for the swollen samples following the protocol described previously in the "Uniaxial compression" section.

Results and discussion

Nanoparticles

TEM images carried out in dried samples (Fig. 2) show that prepared ferrofluids are constituted by roughly spherical, highly crystallized, and almost uniform in size MNPs. The average core diameter of MNPs was determined from the recorded TEM images by counting 200 MNPs considered to be spherical and fitted with a log-normal distribution as shown in Fig. 3. The mean diameter was found 8.1±1.4 nm.

The mean hydrodynamic diameter (D_H) is also obtained by adjusting the experimental data obtained by DLS (see the

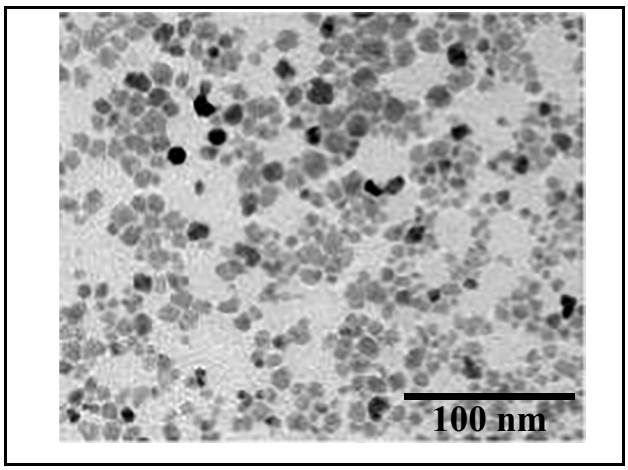

Fig. 2 TEM image of dried MNPs

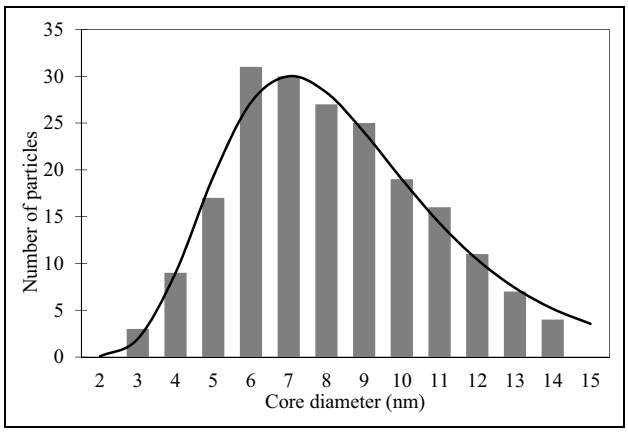

Fig. 3 Core diameter distribution of dried MNPs. The solid line corresponds to the fitting with log normal distribution

"Zeta potential and size distribution by dynamic light scattering (DLS)" section) assuming a monomodal log-normal distribution ($D_H = 9.5 \pm 3.1$ nm). The value is slightly higher than the core diameter determined by TEM (8.1±1.4 nm) proving the stable colloidal state of MNPs in pure water provided by the adsorbed citrated ions. The slight increase is explained by the presence of citrated ions and roughness in the surface of the MNPs. The determined zeta potential (ζ) in a diluted ferrofluid with $\Phi_{MNPs} = 0.2\%$ w/w and pH = 7 was found to be $\zeta = -48.4 \pm 6.2$ mV, a strongly negative value that represents enough surface charge to ensure the strong electrostatic repulsions between MNPs necessary to obtain nanoscale stable colloidal ferrofluid.

Magnetization

Results of magnetization (M) versus applied magnetic field (H) are presented on Fig. 4 for dried MNPs, nanocomposite solutions, and hydrogel for two Φ_{MNPs}. All the results are normalized by the respective Φ_{MNPs}. For dried MNPs, Φ_{MNPs} is calculated considering the 4% w/w of humidity determined by thermogravimetric analysis and the volume masses ($\rho_{H_2O} = 1$ g cm^{-3} and $\rho_{Fe_2O_3} = 5.14$ g cm^{-3}). Two differentiated regions can be clearly observed for the magnetic field dependence of the magnetization for all studied samples. When the magnetic field is increased, the magnetization increases sharply and then tends to a constant value. The low-field measurements in the linear region (see insert of Fig. 4) enable the determination of the initial magnetic susceptibility (χ_0) and the dipolar interaction parameter (γ) with Eqs. 3 and 4. High-field magnetization allows us to determine the saturation magnetization (M_S) of the MNPs.

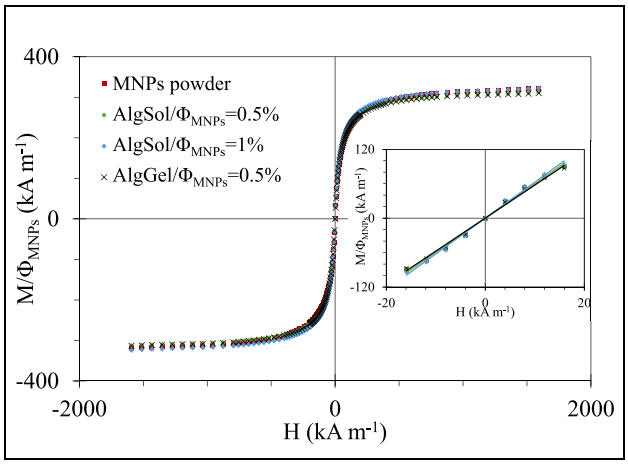

Fig. 4 Magnetization normalized by Φ_{MNPs} as a function of applied magnetic field for dried citrated maghemite MNPs, nanocomposite solutions, and hydrogel. The linear regression at a small value of the magnetic field to determine the magnetic susceptibility (χ_0) is shown in the insert

$$\frac{M}{\Phi_{MNPs}/100} = \chi_0 . H \tag{3}$$

$$\gamma = 3 * \chi_0 \tag{4}$$

The values of magnetization normalized by Φ_{MNPs} obtained for dried MNPs, nanocomposite solutions, and hydrogel (Table 1) are always slightly smaller than the one of bulk maghemite (375 kA m^{-1}) that could be explained either by the estimation of the density of maghemite in the dried powders containing 8–10% w/w sodium citrate which is not considered or by the decrease of the magnetization for very small MNPs due to the prevalence of surface effects as observed in the literature (Tartaj et al. 2003; Lu et al. 2006). It is important to remark that the determined M_S and therefore the behavior of MNPs at high magnetic fields is the same independently of the dispersion in nanocomposites with different Φ_{MNPs} or in sol or hydrogel state demonstrating that the magnetic properties of MNPs are not degraded during the elaboration of the nanocomposites. The obtained values of the dipolar interaction parameter (γ) in the case of dispersions (Table 1) are always smaller than 36 meaning that there is no chaining of the nanoparticles in the samples at zero magnetic field (Huang et al. 2005).

Study of sol-gel transition

Calcium alginate hydrogels

An example of the time evolution of G''/G' at different frequencies from a TRMS experiment just after the addition of GDL for $R_{Ca} = 0.2$ is presented in Fig. 5 including the time evolution of the elastic $G'(t)$ and loss $G''(t)$ moduli for a fixed frequency $f = 1$Hz in the insert. The time evolution of G' and G'' does not allow to define unambiguously the gel point (the crossover could depend on frequency) but it reflects the different steps occurring after the addition of GDL to induce the increase of the amount of dissolved calcium (Ca^{2+}) and the ionic crosslinking of the sodium alginate chains. During a first short step, $G'(t)$ remains nearly constant until an induction time (t_i) from which

Table 1 Magnetic properties of MNPs and nanocomposite solutions and hydrogel

Sample	Φ_{MNPs} (% v/v)	M_s/Φ_{MNPs} (kA m^{-1})	γ (-)
MNP powder	82	322	-
Nanocomposite solution	0.5	313	17.9
Nanocomposite solution	1	323	18.8
Nanocomposite hydrogel	0.5	310	17.3

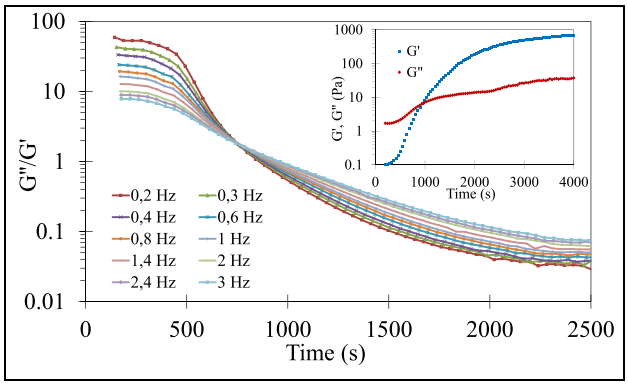

Fig. 5 G''/G' as a function of time at different frequencies for alginate hydrogels with $R_{Ca} = 0.2$. The insert shows the time evolution of G' and G'' at 1Hz

there is enough Ca^{2+} to create the first ionic crosslinks between alginate chains that are detected by the onset of $G'(t)$. Afterwards, the progressive increase of the Ca^{2+} dissolved from the $CaCO_3$ leads to more ionic interactions with the carboxylate groups of first guluronate and then manuronate sequences of the sodium alginate leading to aligned ribbon-like assemblies with cavities in which Ca^{2+} cations are located in the well-known egg-box structure (Grant et al. 1973). This progressive formation of junction zones confirmed experimentally by small angle X-ray scattering measurements (Stokke et al. 2000) induces a sharp increase of $G'(t)$ characteristic of a sol-gel transition and finally at longer time $G'(t)$ tends to nearly constant value G'_∞ considered as a preliminary characterization of the totally gelled state. This description is supported by the addition of $CaCO_3$ powder in the aqueous solution of sodium alginate rapidly leading to a pH = 9 that blocks the dissolution of more $CaCO_3$. Then, by the addition of GDL, the release of protons from the GDL hydrolysis gradually liberates Ca^{2+} from the $CaCO_3$ salt as the following reaction mechanism:

$$CaCO_3(s) \rightarrow Ca^{2+} + CO_3^{2-}$$

$$CO_3^{2-} + H_2O \rightarrow HCO_3^- + OH^-$$

As shown in Fig. 5, the sol-gel transition is studied in more detail by TRMS defining the gelation time (t_g), the gel stiffness (S), and the relaxation exponent (Δ) by the crossover point of G''/G' at different frequencies as firstly proposed by Winter and Chambon (Chambon and Winter 1987). The transition between a liquid-like behavior (G''/G' decreases with the frequency) and solid-like behavior (G''/G' increases with the frequency) can be also observed in this plot.

The results of the TRMS analysis for the calcium alginate hydrogels elaborated with different amounts of calcium ($R_{Ca} = 0.2$, 0.3, and 0.4) are collected in Table 2. We have also included the time of crossover (t_c) of time evolution of G' and G'' and the value of G' at t_c (G'_c) in both cases for $f = 1$Hz. The expected decrease of gelation time (t_g) as R_{Ca} is increased can be explained by the bigger amounts of insoluble calcium dispersed in the pre-gel system as R_{Ca} is increased and the selection of a fixed molar ratio [GDL]/[$CaCO_3$] = 2. For the higher R_{Ca}, the dissolution of $CaCO_3$ is much faster leading to not measurable induction time (t_i). The same tendencies are observed for t_c with higher values than t_g as expected for soft hydrogels (Δ>0.5). Indeed, the differences between t_c which may depend on frequency and t_g become more important when the hydrogels are softer (higher Δ) underlying the interest of the TRMS study experiment and a frequency-independent study of sol-gel transition.

Concerning the characterization of the critical hydrogels (hydrogels at t_g), the increase of R_{Ca} leads to harder critical hydrogels (lower Δ and higher S). Many theoretical models have been proposed to describe a universal behavior of crosslinking polymers at the gel point (Winter and Mours 1997). For example, the Rouse limit without hydrodynamic interactions gives $\Delta = 0.66$, the Zimm limit with hydrodynamic interactions gives $\Delta = 1$, and the percolation model of an electrical network gives $\Delta = 0.71$. It was found experimentally that the gelation induced by chemical crosslinking seems to be well described by the theoretical value of the percolation model which is predicted to be independent of physicochemical conditions (Adolf et al. 1990; Takahashi et al. 1994) while for physical gelation, this universality is not always observed due to the transient nature of the physical crosslinking (Lu et al. 2006; Dai et al. 2010; Liu et al. 2016). For example, values of Δ were experimentally determined between 0.66 and 0.76 depending on the sodium alginate concentration (Liu et al. 2016) using $CaCl_2$ or values between 0.56 and 0.69 (Liu et al. 2003; Lu et al. 2006)

Table 2 Sol-gel transition parameters (t_g, Δ, S) obtained by TRMS and estimated long-time elastic modulus (G'_∞) of calcium alginate hydrogels elaborated with different R_{Ca}

R_{Ca}	t_c (s)	G'_c (Pa)	G'_∞ (Pa)	t_g (s)	Δ	S (Pa s^Δ)
0.2	940±20	6.4±0.9	880	780±10	0.68±0.01	0.54±0.05
0.3	510±20	6.8±0.8	1215	435±5	0.65±0.01	0.68±0.06
0.4	420±20	8.5±1.6	1580	380±10	0.59±0.01	1.56±0.14

depending on the molecular structure of the sodium alginate using $CaCl_2$-EDTA complex. The R_{Ca} dependence of Δ observed in the present study could be explained by a hierarchical gelation due to the inhomogeneity of the sample at the microscopic level considering that the calcium is initially in the form of microparticles of $CaCO_3$. Then, a gradient of Ca^{2+} concentration could appear from those particles inducing the loss of random crosslinking process. In these conditions, the crosslinking of alginate chains will be more important in the regions close to the $CaCO_3$ microparticles leading to a deviation from the theoretical prediction of the percolation model. The effect of these gradients becomes more important for the faster gelation that could explain the difference between experimental (Table 2) and theoretical ($\Delta = 0.71$) values of Δ increase when R_{Ca} is increased (t_g decrease). Concerning G'_∞, the values increase as R_{Ca} is increased in good agreement with the behavior at t_g (lower values of Δ and higher values of S).

Calcium alginate nanocomposite hydrogels

Effect of Φ_{MNPs} The results of the TRMS analysis presented in Table 3 show that the addition of MNPs induces an increase of the gelation time by a factor of 1.3 for the lower content of MNPs ($\Phi_{MNPs} = 0.5\%$) and by a factor of 5 for the higher content of MNPs ($\Phi_{MNPs} = 1\%$). The nanocomposites have also values of Δ and S characteristic of softer critical gels than the calcium alginate hydrogel prepared with the same conditions.

Both the slowdown of sol-gel transition kinetics and the softer critical hydrogels could be related to interactions between Ca^{2+} and citrated MNPs. The citrate anions of MNPs can bind calcium of the aqueous phase displacing the calcium carbonate equilibrium and consequently decreasing available Ca^{2+} to crosslink ionically the sodium alginate chains as reported by Mekmene et al. (2011). This effect is in good agreement with the previously observed effect of R_{Ca} on calcium alginate hydrogels leading to softer critical gels for lower R_{Ca} corresponding with slower gelation rates. As well as for the different R_{Ca}, no universal Δ value can be observed when the sol-gel transition kinetics are modified by the addition of MNPs. These results are in good agreement with the conjecture of not universal Δ in physical gelation but strongly dependent on the microstructure and the route to achieve the critical point (Suman and Joshi 2020). For the present case, the bigger differences of the experimentally obtained Δ and the one predicted by the percolation model could be explained by a more random gelation for the slower kinetics. Moreover, the introduction of MNPs has also an effect in the values of G'_∞ that seems to change independently of the critical gel properties. The value of G'_∞ is not affected with $\Phi_{MNPs} = 0.5\%$ while $\Phi_{MNPs} = 1\%$ leads to an important decrease.

Effect of an applied magnetic field As showed in a previous study (Roger et al. 2015), the application of a magnetic field modifies the viscoelastic properties of the elaborated nanocomposites in sol state due to the elongation in the direction of the field of a microstructure composed of droplets of phase separation. Thus, the purpose is now to evaluate if this magneto-induced structural modification allows to modulate the sol-gel transition and therefore the obtained properties of the nanocomposite hydrogels. The selected samples for this study are the calcium alginate nanocomposite hydrogels with $R_{Ca} = 0.4$ prepared with two volume fractions of MNPs ($\Phi_{MNPs} = 0.5\%$ and $\Phi_{MNPs} = 1\%$) and the applied magnetic fields of 2.6, 6.7, and 13.9 kA m^{-1} were homogeneous and perpendicular to the shear stress.

A preliminary analysis is performed by plotting the time evolution of the viscoelastic moduli G′ and G″ (Fig. 6) at a fixed frequency (1 Hz). An enhancement of G′ before the crossover of both moduli (t_c) is clearly observed by the application of a magnetic field that could be explained by the deformation of droplets of phase separation along the direction of the magnetic field as observed in nanocomposite solutions (Roger et al. 2015). For $t > t_c$, we could expect that the deformation of droplets is hindered by the three-dimensional network of the hydrogel leading to no noticeable effects of the magnetic field on G′ and G″. The results for a magnetic field of 13.9 kA m^{-1} are not presented here since the magnetic effect is high enough to change the material at the initial state into a viscoelastic solid (G′>G″) hindering the observation of the sol-gel transition induced by the crosslinking with Ca^{2+}. For the other volume fraction ($\Phi_{MNPs} = 0.5$ %), similar magnetic effects but considerably weaker due to the lower content of MNPs have been found. The results are not shown here for brevity.

The TRMS results were analyzed applying the methodology shown previously obtaining the parameters summarized in Table T1 in the supporting information for

Table 3 Results of the study of the sol-gel transition of nanocomposites with $R_{Ca} = 0.4$ and different volume fractions of MNPs

Φ_{MNPs} (%)	t_c (s)	G'_c (Pa)	G'_∞ (Pa)	t_g (s)	Δ	S (Pa s^{Δ})
0	420±20	8.5±1.6	1215	380±10	0.59±0.01	1.56±0.14
0.5	530±20	8.6±1.4	1260	525±10	0.63±0.02	0.93±0.11
1	2030±20	8.5±0.5	345	1870±25	0.67±0.03	0.86±0.15

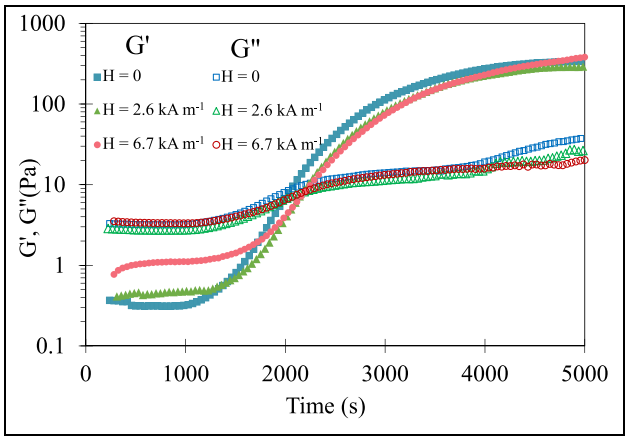

Fig. 6 Evolution of G′ and G″ as a function of time for a $f = 1$ Hz for alginate nanocomposite hydrogels with $R_{Ca} = 0.4$ and Φ_{MNPs}=1% during the application of the magnetic field of different values

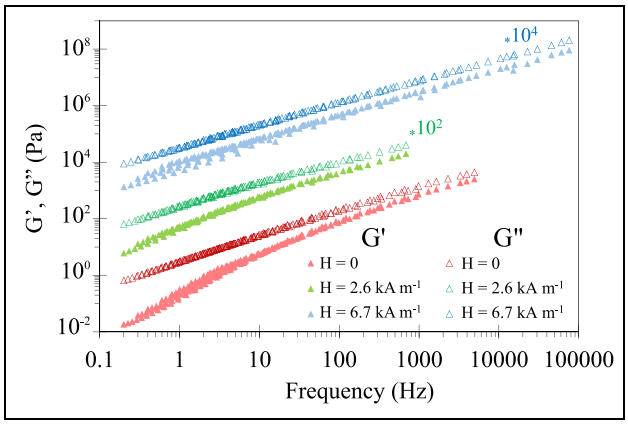

Fig. 7 Master curve of G′ and G″ of nanocomposite hydrogels with R_{Ca}=0.4 and Φ_{MNPs} = 1% obtained from the shifting and superposition of data of G′(*f*) and *G″*(*f*) before the gel point without and with the application of magnetic field

both volume fractions (Φ_{MNPs}=0.5% and Φ_{MNPs}=1%) and the three values of applied magnetic fields. Unexpectedly, the applied magnetic field has no clear effect on the parameters S and Δ of the critical hydrogel even if the viscoelastic properties are enhanced before the gel point as it has been shown in Fig. 6. This suggests that the deformation of droplets of phase separation induced by a moderate magnetic field ($H \leq 13.9$ kA m^{-1}) do not influence the three-dimensional network of the critical hydrogel.

Considering the similar shape of the curves of $G'(f)$ and $G''(f)$ at different times (Figs. S2, S3, and S4 in the supporting information), a master curve could be built as proposed by Hodgson (Hodgson and Amis 1990). For this purpose, G′ and G″ are shifted vertically and horizontally by factors α_v and α_h.

$$\alpha_v = \left(\frac{\epsilon}{\epsilon_r}\right)^n \tag{5}$$

$$\alpha_h = \left(\frac{\epsilon}{\epsilon_r}\right)^m \tag{6}$$

$$n = -k \tag{7}$$

$$m = -(k+z) \tag{8}$$

$$\Delta = \frac{z}{k+z} \tag{9}$$

where ϵ_r is the value of the relative distance to the gel point ($\epsilon_r = (t_g - t_r)/t_g$). The parameters n and m are related to the critical exponent for the zero-shear viscosity (k) at $t < t_g$ and the critical exponent for the equilibrium modulus (z) at $t \geq t_g$. The critical exponent z was determined from the value of G' extrapolated to zero-frequency quenching the sol-gel transition by some authors (Liu et al. 2016). For the present study, we did not use this strategy for this determination of z since it is not possible to quench the sol-gel transition and the measurements of G′ at lower frequencies require too long experimental time in comparison with the time evolution of the viscoelastic properties. Then, both z and k have been considered as free parameters to obtain the best adjustment of the master curve. The good adjustment of the data confirms the self-similar structure of the nanocomposites leading to a master curve over at least five decades of frequency (Fig. 7). In addition, the determination of the exponents z and k allows to determine Δ postulating a symmetry of the divergence on both sides of the gel point (Eq. 9).

The results of the adjusted values of z and k as well as the deduced values of Δ from Eq. 9 are summarized in Table T1 in the supporting information. As stated previously for Δ, the critical exponents z and k can be predicted by different theoretical models. For example, the Rouse limit without hydrodynamic interaction gives $z = 2.7$ and $k = 1.35$, while the values for the Zimm limit with hydrodynamic interaction are $z = 2.7$ and $k = 0$. The percolation model of an electrical network yields to $z = 1.94$ and $k = 0.75$. However, the universality of these exponents has been questioned by the several experimental values of k and z found in the literature. For calcium alginate hydrogels, the values of z and k were evaluated by two complementary methodologies (Lu et al. 2006) finding two different behaviors: (1) for alginate with lower molecular weight, critical exponents were almost independent of alginate concentration and close to the percolation prediction and (2) for the alginate with higher molecular weight, the critical exponents change with the concentration and type of alginate.

As observed in Table T1 in the supporting information, the values of the parameters z, k, and Δ obtained from the master curve adjustment are globally close to the ones of the percolation model of an electrical network. The main differences are found for the sample with the higher Φ_{MNPs} and $H = 6.7$ kA m^{-1} with higher values for both z and k. This discrepancy could be related with the clear increase of G′ before the gel point observed in Fig. 6.

Characterization of totally gelled hydrogels

Calcium alginate and nanocomposite hydrogels prepared as described in the "Study of totally gelled hydrogels" section were analyzed in order to study their viscoelastic (shear rheology and uniaxial compression) and swelling properties.

Shear rheology

The strain amplitude dependence of the elastic (G') and viscous (G'') moduli in hydrogel and nanocomposite hydrogels are presented in Fig. 8. From these curves, critical strains (γ_c) defined from the onset of decrease of the elastic modulus (G′), mean values of G′ in the LVD (G'_{LVD}), strain at the peak of G″ (γ''), and maximum value of G″ (G''_{max}) were calculated and summarized in Table T2 of the supporting information. All the investigated samples have an elastic component (G′) dominating over the viscous component (G″) in the LVD confirming a solid viscoelastic gel network.

The results for nanocomposite hydrogels show a decrease of G'_{LVD} and an increase of the critical strains (γ_c and $\gamma_{''max}$) as Φ_{MNPs} is increased. Thus, the addition of MNPs allows to obtain more flexible hydrogel networks that can resist higher deformations before losing their structures in good agreement with the decrease of the mechanical properties observed in the previous study of the sol-gel transition (G'_∞ in Table 3). This is probably due to the electrostatic interactions between Ca^{2+} and the negatively charged citrate ions of the MNPs (Mekmene and Gaucheron 2011). The presence of a peak with a clearly identified maximum for G″ has also been observed in other nanocomposites (Santos et al. 2018; Marić et al. 2020; Porter et al. 2021) and related with the energy dissipation due to the breakage of the gel-like structure (Santos et al. 2018). In the present case, the presence of a peak at higher γ″ in nanocomposites than in polymer hydrogels suggests that the presence of MNPs gives rise to a microstructure that results in a higher resistance to the flow inside the sample in good agreement with the microstructure of droplets of phase separation observed by optical microscopy in a previous study in nanocomposite solutions (Tarrío-Saavedra et al. 2017). However, no significant tendency of G''_{max} is found when the value of Φ_{MNPs} is increased.

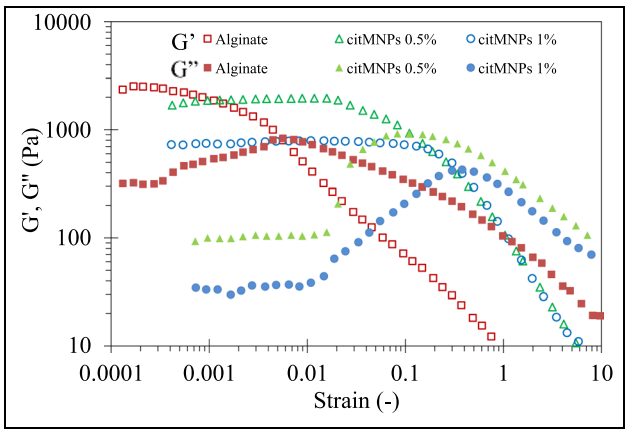

Fig. 8 Elastic (G′) and viscous (G″) moduli as a function of the strain amplitude for hydrogel and nanocomposite hydrogels with $C_{alg} = 18$ g L^{-1}, $R_{Ca} = 0.4$, and two Φ_{MNPs}

Uniaxial compression

The stress-strain curves of uniaxial compression measurements in the linear domain performed for identical samples than those studied by shear rheology are presented in Fig. 9. The uniaxial compressive Young modulus (E) can be deduced as the slope by a linear fit of experimental data at low strain. A strain hardening effect is observed at strain values higher than 0.08. This stiffening as strain is increased is commonly observed in polysaccharide hydrogels and other biological tissues (Furlani et al. 2021). For the case of polyelectrolyte hydrogels, it was attributed to the formation of a stiffer percolation structure due to the strain-induced ionic clustering (Miquelard-Garnier et al.

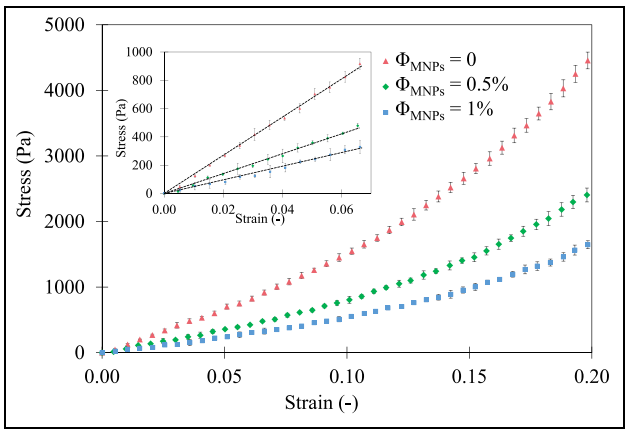

Fig. 9 Stress-strain uniaxial compression curves for hydrogel and nanocomposite hydrogels with $C_{alg} = 18$ g L^{-1}, $R_{Ca} = 0.4$, and two Φ_{MNPs}. Each point corresponds to an average between 3 independent experiments with their standard deviation represented by an error bar. The insert shows the linear region. The lines correspond to a linear regression of experimental data

Table 4 Degree of syneresis for hydrogel and nanocomposite hydrogels with $C_{alg} = 18$ g L^{-1}, $R_{Ca} = 0.4$, and two Φ_{MNPs}

Φ_{MNPS}(%)	Degree of syneresis (%)
0	13.7
0.5	3.3
1	0.4

2008). The viscoelastic properties presented previously and the compressive properties show similar trends. Adding MNPs decreases the compressive Young modulus (see Fig. 9) in agreement with the decrease of the value of G'_{LVD} determined by shear rheology (the "Shear rheology" section). This correlation between shear and compressive mechanical properties is in a good agreement with other studies of nanocomposites (Yu et al. 2018; Cai et al. 2020).

Syneresis

The results of the degree of syneresis of hydrogel and nanocomposite hydrogels measured as the relative difference of mass between the pre-gel and the as-prepared hydrogel at $t = 16$ h are summarized in Table 4.

This irreversible time-dependent de-swelling of hydrogels or syneresis is due to local shrinkage of the three-dimensional network and consequently is related with the structure, the porosity, and the mechanical properties of the hydrogels. In case of calcium alginate hydrogels ionically crosslinked by interactions of negatively charged COO^- with Ca^{2+}, Draget et al. (2001) showed by small angle X-ray scattering that syneresis can be related to an increase of the lateral association of junction zones depending on chain flexibility, guluronic content and the molecular weight. The decrease of the degree of syneresis when the amount of MNPs is increased obtaining a more porous network is in good correlation with the decrease of mechanical properties (viscoelastic and compressive Young moduli).

Swelling

Swelling of hydrogels is a complex process that comprises several steps from an initial dried hydrogel to a swollen hydrogel. The time evolution of the degree of swelling measured for as-prepared hydrogels at identical conditions than those studied by shear rheology and uniaxial compression is presented in Fig. 10. For all studied samples, the degree of swelling increases rapidly during an initial step and then slows down to reach an equilibrium swelling state (Q_e). Two kinetic models are commonly used in the literature (Simonin 2016) for the modeling of absorption kinetics:

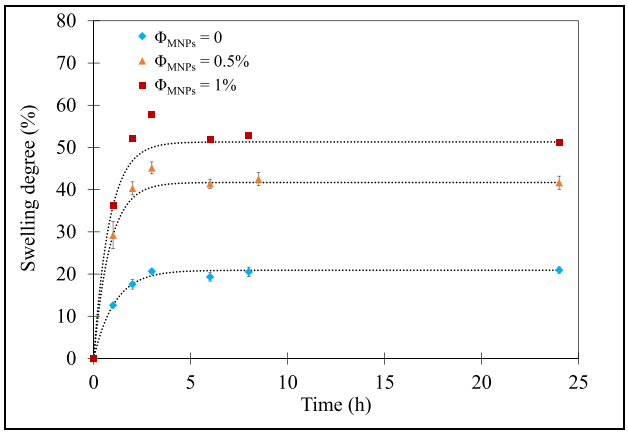

Fig. 10 Time evolution of the swelling degree for calcium alginate nanocomposite hydrogels with $R_{Ca} = 0.4$ and two Φ_{MNPs}. The dashed lines correspond to the fitting of experimental data with the first-order kinetic model (Eq. 10)

$$Pseudo\ first-order\ model: Q(t) = Q_e.\left(1 - e^{-k_1.t}\right) \quad (10)$$

$$Pseudo\ second-order\ model: Q(t) = Q_e.\frac{k_2.t}{1 + k_2.t} \quad (11)$$

where k_1 and k_2 are the pseudo first-order and second-order constants respectively.

Considering that a significant number of experimental points (at least 50%, Fig. 10) are close to equilibrium, it was shown (Simonin 2016) that a fitting with two open parameters (Q_e and k_1 or k_2) may introduce errors. Consequently, Q_e are fixed to experimental values and the constants k_1 or k_2 are the only open parameters for the adjustment. Experimental data were fitted by the two kinetic models (Eqs. 10 and 11) and the best fitting was obtained by the first-order model (Eq. 10, Fig. 10). The results are summarized in Table T3 in the supporting information. By the immersion of the hydrogels in water, the diffusion of water into the network takes place driven by the high hydrophilicity of alginate. This swelling is governed by the balance between the stretching produced by the volume expansion and the elastic contraction produced by the chains of alginate. At low times, an increase of the slope of the swelling curve is clearly observed for the composite hydrogels in comparison to hydrogels without MNPs (Fig. 10). This indicates a faster rate of water absorption. This promoted water diffusion in composite hydrogels of softer structure (decrease of G'_{LVD} and E) compared to hydrogels without MNPs could be related to higher space for water absorption and weaker contraction forces against volume expansion.

It should be underlined that the kinetic model does not take into account of overshooting effect observed near

the swelling equilibrium for composite hydrogels. This phenomenon was observed for other hydrogels (Yin et al. 2008). Firstly, it was explained by a relaxation process of the macromolecular chains (Shieh and Peppas 1991). Later, this behavior was related to the presence of osmolytes (low molecular weight organic compounds that influence the solvent quality when they penetrate in the hydrogel network) (Aangenendt et al. 2020). Since this overshooting effect is observed only for nanocomposites, a first explanation could be that citrated ions of MNPs or the MNPs themselves play the role of osmolytes that induce the observation of this maximum swelling. Recently, a mathematical model has been developed by Bisotti et al. (2022) that accurately fits this overshooting for polyacrylic-based hydrogels. However, the limited experimental data and studied conditions of this work do not allow to adjust the five parameters of this model.

Uniaxial compression of swollen disks

The compressive properties of the nanocomposite hydrogels depend on their swelling state showing a significantly higher compressive Young modulus at the swollen equilibrium (E_{sw}) than for as-prepared samples (E) as shown in Fig. 11. This increase of the compressive Young modulus is related with the quantity of absorbed water that penetrates in the pores of the hydrogel elongating the alginate chains and stiffening the network. The ratio of increase of the Young modulus (E_{sw}/E) is correlated with the amount of water absorbed during the swelling. Higher volume fractions of MNPs lead to higher chain flexibility allowing a higher amount of water absorbed inducing a more important increase of the Young modulus (ratio E_{sw}/E).

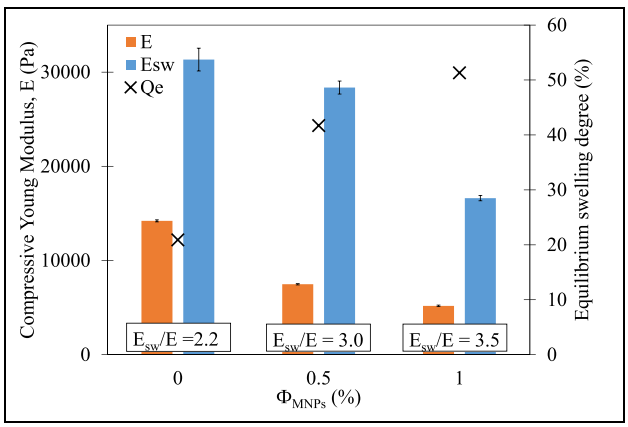

Fig. 11 Equilibrium swelling degree (Q_e) and compressive Young modulus of swollen in comparison to as-prepared hydrogel and nanocomposite hydrogels with $R_{Ca} = 0.4$ and two Φ_{MNPs}

Conclusions

New magnetic sensitive nanocomposite hydrogels with tunable mechanical and swelling properties have been elaborated by the addition of citrated magnetic nanoparticles (MNPs) in a sodium alginate aqueous solution ionically crosslinked by in situ calcium release from insoluble calcium carbonate ($CaCO_3$) salt. This work provides a comprehensive study of their viscoelastic and swelling properties in relation to their elaboration. The sol-gel transition has been firstly investigated by time-resolved mechanical spectroscopy (TRMS) by varying the amount of added calcium, the volume fraction of MNPs (Φ_{MNPs}), and the applied magnetic field (H). The results show an expected slowdown of the kinetic gelation process (decrease of gelation time t_g) and softer critical hydrogels by decreasing the amount of calcium or increasing Φ_{MNPs}. In this later case, it could be explained by the calcium-binding capacity of citrate used to stabilize MNPs. Elastic moduli of nanocomposites at constant Φ_{MNPs} could be increased until t_g by applying and increasing H. However, no noticeable H effect is observed in critical hydrogels suggesting that the deformation of droplets of phase separation induced by a moderate magnetic field ($H \leq 13.9$ kA m^{-1}) does not modify the three-dimensional network of the critical hydrogel. Before the gel point (time $< t_g$), the storage G′ and loss G″ moduli obtained at various relative distances to the gel point can be superposed fairly well to form a master curve. The critical exponents of the scaling laws for zero shear viscosity before the gel point (time $< t_g$) and the equilibrium modulus after the gel point (time $> t_g$) were evaluated from the shift factors and found globally close to the ones predicted by percolation theory of an electrical network.

Viscoelastic and mechanical properties of totally gelled nanocomposites have been secondly studied by shear rotational rheology and uniaxial compressive tests as well as swelling properties by water immersion. The linear viscoelastic moduli and compressive Young modulus of hydrogels with MNPs are lower than the ones for hydrogels without MNPs. Higher content of MNPs also resulted in a significant decrease of syneresis, softer nanocomposites promoting water diffusion, and increased equilibrium swelling degree deduced from swelling kinetics fitted by a first-order kinetic model.

Supplementary Information The online version contains supplementary material available at https://doi.org/10.1007/s00397-023-01384-1.

Declarations

Competing interests The authors declare no competing interests.

References

Aangenendt FJ, Punter MTJJM, Mulder BM et al (2020) Nonmonotonic swelling and compression dynamics of hydrogels in polymer solutions. Phys Rev E 102:062606. https://doi.org/10.1103/PhysRevE.102.062606

Adolf D, Martin JE, Wilcoxon JP (1990) Evolution of structure and viscoelasticity in an epoxy near the sol-gel transition. Macromolecules 23:527–531. https://doi.org/10.1021/ma00204a028

Ahn S, Kasi RM, Kim S-C et al (2008) Stimuli-responsive polymer gels. Soft Matter 4:1151–1157. https://doi.org/10.1039/B714376A

Bisotti F, Pizzetti F, Storti G, Rossi F (2022) Mathematical modelling of cross-linked polyacrylic-based hydrogels: physical properties and drug delivery. Drug Deliv and Transl Res 12:1928–1942. https://doi.org/10.1007/s13346-022-01129-2

Cai Z, Wu J, Wu M et al (2020) Rheological characterization of novel carboxymethylated curdlan-silica hybrid hydrogels with tunable mechanical properties. Carbohydr. Polym. 230:115578. https://doi.org/10.1016/j.carbpol.2019.115578

Chambon F, Winter HH (1987) Linear viscoelasticity at the gel point of a crosslinking PDMS with imbalanced stoichiometry. J Rheol 31:683–697. https://doi.org/10.1122/1.549955

Dai L, Liu X, Tong Z (2010) Critical behavior at sol–gel transition in gellan gum aqueous solutions with KCl and CaCl2 of different concentrations. Carbohydr. Polym. 81:207–212. https://doi.org/10.1016/j.carbpol.2010.02.013

Dos STC, Hernández R, Rescignano N et al (2018) Nanocomposite chitosan hydrogels based on PLGA nanoparticles as potential biomedical materials. Eur. Polym. J. 99:456–463. https://doi.org/10.1016/j.eurpolymj.2017.12.039

Draget KI, Taylor C (2011) Chemical, physical and biological properties of alginates and their biomedical implications. Food Hydrocoll. 25:251–256. https://doi.org/10.1016/j.foodhyd.2009.10.007

Draget KI, Gåserød O, Aune I et al (2001) Effects of molecular weight and elastic segment flexibility on syneresis in Ca-alginate gels. Food Hydrocoll. 15:485–490. https://doi.org/10.1016/S0268-005X(01)00046-7

Furlani F, Marfoglia A, Marsich E et al (2021) Strain hardening in highly acetylated chitosan gels. Biomacromolecules 22:2902–2909. https://doi.org/10.1021/acs.biomac.1c00293

Galindo-Gonzalez C, Ponton A, Bee A et al (2016) Investigation of water-based and oil-based ferrofluids with a new magnetorheological cell: effect of the microstructure. Rheol. Acta 55:67–81. https://doi.org/10.1007/s00397-015-0892-5

George J, Ishida H (2018) A review on the very high nanofiller-content nanocomposites: their preparation methods and properties with high aspect ratio fillers. Prog. Polym. Sci. 86:1–39. https://doi.org/10.1016/j.progpolymsci.2018.07.006

Grant GT, Morris ER, Rees DA et al (1973) Biological interactions between polysaccharides and divalent cations: the egg-box model. FEBS Lett. 32:195–198. https://doi.org/10.1016/0014-5793(73)80770-7

Growney Kalaf EA, Flores R, Bledsoe JG, Sell SA (2016) Characterization of slow-gelling alginate hydrogels for intervertebral disc tissue-engineering applications. Mater Sci Eng C Mater Biol Appl 63:198–210. https://doi.org/10.1016/j.msec.2016.02.067

Hodgson DF, Amis EJ (1990) Dynamic viscoelastic characterization of sol-gel reactions. Macromolecules 23:2512–2519. https://doi.org/10.1021/ma00211a019

Huang JP, Wang ZW, Holm C (2005) Computer simulations of the structure of colloidal ferrofluids. Phys Rev E 71:061203. https://doi.org/10.1103/PhysRevE.71.061203

Hunter RJ (1981) COLLOID SCIENCE. In: Zeta potential in colloid science. Academic Press, p ii

Ingar Draget K, Østgaard K, Smidsrød O (1990) Homogeneous alginate gels: a technical approach. Carbohydr. Polym. 14:159–178. https://doi.org/10.1016/0144-8617(90)90028-Q

Kaszuba M, Corbett J, Watson FM, Jones A (2010) High-concentration zeta potential measurements using light-scattering techniques. Philos Trans A Math Phys Eng Sci 368:4439–4451. https://doi.org/10.1098/rsta.2010.0175

Leong J-Y, Lam W-H, Ho K-W et al (2016) Advances in fabricating spherical alginate hydrogels with controlled particle designs by ionotropic gelation as encapsulation systems. Particuology 24:44–60. https://doi.org/10.1016/j.partic.2015.09.004

Li J, Wu Y, He J, Huang Y (2016) A new insight to the effect of calcium concentration on gelation process and physical properties of alginate films. J Mater Sci 51:5791–5801. https://doi.org/10.1007/s10853-016-9880-0

Liu X, Qian L, Shu T, Tong Z (2003) Rheology characterization of sol–gel transition in aqueous alginate solutions induced by calcium cations through in situ release. Polymer 44:407–412. https://doi.org/10.1016/S0032-3861(02)00771-1

Liu S, Li H, Tang B et al (2016) Scaling law and microstructure of alginate hydrogel. Carbohydr. Polym. 135:101–109. https://doi.org/10.1016/j.carbpol.2015.08.086

Lu L, Liu X, Tong Z, Gao Q (2006) Critical exponents and self-similarity for sol-gel transition in aqueous alginate systems induced by in situ release of calcium cations. J Phys Chem B 110:25013–25020. https://doi.org/10.1021/jp060155e

Maki Y, Ito K, Hosoya N et al (2011) Anisotropic structure of calcium-induced alginate gels by optical and small-angle X-ray scattering measurements. Biomacromolecules 12:2145–2152. https://doi.org/10.1021/bm200223p

Marić I, Vujičić NŠ, Pustak A et al (2020) One-step synthesis of poly(ethylene oxide)/gold nanocomposite hydrogels and suspensions using gamma-irradiation. Radiat. Phys. Chem. 170:108657. https://doi.org/10.1016/j.radphyschem.2019.108657

Massart R (1982) Majestic fluids and process for obtaining them. Ronay, IBM Tech. Disclosure Bull 19(7):2753–2758

Mekmene O, Gaucheron F (2011) Determination of calcium-binding constants of caseins, phosphoserine, citrate and pyrophosphate: a modelling approach using free calcium measurement. Food Chem. 127:676–682. https://doi.org/10.1016/j.foodchem.2010.12.121

Miquelard-Garnier G, Creton C, Hourdet D (2008) Strain induced clustering in polyelectrolyte hydrogels. Soft Matter 4:1011–1023. https://doi.org/10.1039/B717460H

Mours M, Winter HH (1994) Time-resolved rheometry. Rheol Acta 33:385–397. https://doi.org/10.1007/BF00366581

Okay O (2010) General properties of hydrogels. In: Gerlach G, Arndt K-F (eds) Hydrogel sensors and actuators: engineering and technology. Springer, Berlin, Heidelberg, pp 1–14

Ostolska I, Wiśniewska M (2014) Application of the zeta potential measurements to explanation of colloidal Cr2O3 stability mechanism in the presence of the ionic polyamino acids. Colloid Polym Sci 292:2453–2464. https://doi.org/10.1007/s00396-014-3276-y

Patel P, Thareja P (2022) Hydrogels differentiated by length scales: a review of biopolymer-based hydrogel preparation methods, characterization techniques, and targeted applications. Eur. Polym. J. 163:110935. https://doi.org/10.1016/j.eurpolymj.2021.110935

Porter GC, Schwass DR, Tompkins GR et al (2021) AgNP/alginate nanocomposite hydrogel for antimicrobial and antibiofilm applications. Carbohydr Polym 251:117017. https://doi.org/10.1016/j.carbpol.2020.117017

Ridi F, Bonini M, Baglioni P (2014) Magneto-responsive nanocomposites: preparation and integration of magnetic nanoparticles into films, capsules, and gels. Adv Colloid Interface Sci 207:3–13. https://doi.org/10.1016/j.cis.2013.09.006

Roger S, Sang YYC, Bee A et al (2015) Structural and multi-scale rheophysical investigation of diphasic magneto-sensitive materials based on biopolymers. Eur Phys J E 38:88. https://doi.org/10.1140/epje/i2015-15088-1

Sakugawa K, Ikeda A, Takemura A, Ono H (2004) Simplified method for estimation of composition of alginates by FTIR. J. Appl. Polym. Sci. 93:1372–1377. https://doi.org/10.1002/app.20589

Sanchez C, Julián B, Belleville P, Popall M (2005) Applications of hybrid organic–inorganic nanocomposites. J Mater Chem 15:3559–3592. https://doi.org/10.1039/B509097K

Sarkar S, Guibal E, Quignard F, SenGupta AK (2012) Polymer-supported metals and metal oxide nanoparticles: synthesis, characterization, and applications. J Nanopart Res 14:715. https://doi.org/10.1007/s11051-011-0715-2

Schexnailder P, Schmidt G (2009) Nanocomposite polymer hydrogels. Colloid Polym Sci 287:1–11. https://doi.org/10.1007/s00396-008-1949-0

Shieh LY, Peppas NA (1991) Solute and penetrant diffusion in swellable polymers. XI. The dynamic swelling behavior of hydrophilic copolymers containing multiethylene glycol dimethacrylates. J. Appl. Polym. Sci. 42:1579–1587. https://doi.org/10.1002/app.1991.070420611

Simonin J-P (2016) On the comparison of pseudo-first order and pseudo-second order rate laws in the modeling of adsorption kinetics. J. Chem. Eng. https://doi.org/10.1016/j.cej.2016.04.079

Stokke BT, Draget KI, Smidsrød O et al (2000) Small-angle X-ray scattering and rheological characterization of alginate gels. 1. Ca−alginate gels. Macromolecules 33:1853–1863. https://doi.org/10.1021/ma991559q

Stuart MAC, Huck WTS, Genzer J et al (2010) Emerging applications of stimuli-responsive polymer materials. Nature Mater 9:101–113. https://doi.org/10.1038/nmat2614

Suman K, Joshi YM (2020) On the universality of the scaling relations during sol-gel transition. J Rheol 64:863–877. https://doi.org/10.1122/1.5134115

Takahashi M, Yokoyama K, Masuda T, Takigawa T (1994) Dynamic viscoelasticity and critical exponents in sol-gel transition of an end-linking polymer. J Chem Phys 101:798–804. https://doi.org/10.1063/1.468135

Tarrío-Saavedra J, González CG, Naya S et al (2017) Statistical modeling applied to deformation-relaxation processes in a composite biopolymer network induced by magnetic field. PLOS ONE 12:e0169866. https://doi.org/10.1371/journal.pone.0169866

Tartaj P, Morales Ma Del P, Veintemillas-Verdaguer S et al (2003) The preparation of magnetic nanoparticles for applications in biomedicine. J Phys D: Appl Phys 36:R182–R197. https://doi.org/10.1088/0022-3727/36/13/202

Thévenot J, Oliveira H, Sandre O, Lecommandoux S (2013) Magnetic responsive polymer composite materials. Chem Soc Rev 42:7099–7116. https://doi.org/10.1039/C3CS60058K

Varaprasad K, Raghavendra GM, Jayaramudu T et al (2017) A mini review on hydrogels classification and recent developments in miscellaneous applications. Mater. Sci. Eng. C 79:958–971. https://doi.org/10.1016/j.msec.2017.05.096

Winter HH, Mours M (1997) Rheology of polymers near liquid-solid transitions. In: Neutron spin echo spectroscopy viscoelasticity rheology. Springer, Berlin, Heidelberg, pp 165–234

Winter HH, Morganelli P, Chambon F (1988) Stoichiometry effects on rheology of model polyurethanes at the gel point. Macromolecules 21:532–535. https://doi.org/10.1021/ma00180a048

Yamamoto K, Yuguchi Y, Stokke BT et al (2019) Local structure of Ca2+ alginate hydrogels gelled via competitive ligand exchange and measured by small angle X-ray scattering. Gels 5:3. https://doi.org/10.3390/gels5010003

Yin Y, Ji X, Dong H et al (2008) Study of the swelling dynamics with overshooting effect of hydrogels based on sodium alginate-g-acrylic acid. Carbohydr. Polym. 71:682–689. https://doi.org/10.1016/j.carbpol.2007.07.012

Yu L, Wang D, Tan Y et al (2018) Super tough bentonite/SiO2-based dual nanocomposite hydrogels using silane as both an intercalator and a crosslinker. Appl. Clay Sci. 156:53–60. https://doi.org/10.1016/J.CLAY.2018.01.026